Proceedings of the 33rd European Safety and Reliability Conference (ESREL 2023)
Edited by Mário P. Brito, Terje Aven, Piero Baraldi, Marko Čepin and Enrico Zio
 Published by Research Publishing, Singapore.
doi: 10.3850/978-981-18-8071-1_P713-cd

Mechanical Performance Analysis of High Pressure Wellhead Based on Thermodynamic Coupling Model

Bin Li

College of Safety and Ocean Engineering, China University of Petroleum(Beijing), China.

Shengnan Wu

College of Safety and Ocean Engineering, China University of Petroleum(Beijing), China. E-mail: wushengnan@cup.edu.cn

Laibin Zhang

College of Safety and Ocean Engineering, China University of Petroleum(Beijing), China.

Qiao Zhang

College of Safety and Ocean Engineering, China University of Petroleum(Beijing), China.

Tianhao Liu

College of Safety and Ocean Engineering, China University of Petroleum(Beijing), China.

ABSTRACT: Due to the effect of harsh environmental factors and huge alternating moment loads, subsea wellhead system is prone to fatigue damage. The high pressure wellhead , as an important component and pressure-bearing part of the subsea wellhead, imposes higher requirements on its safety performance under the complex temperature-pressure coupling environment. A comprehensive assessment of the safety performance of key pressure-bearing components in subsea wellhead is crucial, but thermodynamic coupling factors are missing in performance analysis of traditional methods. This paper proposes a safety performance analysis method of the high pressure wellhead, which combines wellbore temperature distribution and location. A coupled finite element model is established for high pressure wellhead thermodynamically analysis, considering the effects of sensitive factors such as bending moment loads and temperature on safety performance. The approach is tested through the application to a case study with a subsea wellhead system in the South China Sea. The results show that the bending moment can cause greater equivalent stress on the pressure bearing components, and the impact on the locking ring is greater than the high-pressure wellhead. Temperature has a particularly significant impact on the casing and locking ring. Compared to traditional subsea wellhead safety performance evaluation methods, the technique proposed can be used for a broader and more comprehensive evaluation of subsea wellhead safety performance, and is more suitable for guidance of practical engineering applications.

Keywords: Subsea Wellhead; Moment load; Temperature; Thermodynamic coupling analysis

1. Introduction

In the process of deepwater offshore oil and gas exploration and development, the high-pressure wellhead is the basic equipment for drilling and oil and gas production facilities, playing a connecting role (Wang et al., 2022). It bears the weight of the casing string, ocean environmental loads, bending moment, well pressure, drilling equipment such as risers and blowout preventers, and production facilities such as Christmas trees (Deng et al., 2019). The subsea wellhead is sensitive to changing in external loads. It is exposed to dynamic loads generated by the marine environment for a long time, fatigue damage on the weak points of the subsea wellhead will continue to accumulate (Liu et al., 2016). Under the effect of temperature, the sealing performance of the subsea wellhead connection structure will be affected and the fatigue accumulation rate will increase (Li et al., 2023). Once the cumulative damage exceeds the fatigue damage limit, the subsea wellhead will generate

failure or even fracture, which may lead to accidents such as blowout (Chang et al., 2019). In the actual analysis process, the model can be appropriately simplified, and the established high-pressure wellhead model usually includes high-pressure wellhead, rigid locking assembly, locking ring, conduit head, casing, conduit, and cement sheath (Wu et al., 2018). At present, many scholars have studied the remaining life and fatigue damage of subsea wellhead. Nonlinear cumulative fatigue model, semi-decoupled model, fully decoupled model, numerical models for analysis stability and fatigue life curve testing scheme for subsea wellhead have been proposed successively (Wang et al., 2022, Li et al., 2020, Qiu et al., 2022, Yan et al., 2015, Anders et al., 2017). The Subsea wellhead remaining life prediction model based on Wiener process, Bayesian network and consideration of temperature and pressure effects improves the accuracy of prediction results, and the practical effect is verified in the example analysis (Cai et al., 2022, Zhang et al., 2021, Meng et al., 2022, Wang et al., 2022). Up to now, the commonly used semi-decoupled models for subsea wellhead have been greatly simplified, which can reduce the calculation amount and effectively avoid the problem of non-convergence of the calculation results. However, such models cannot conduct further research on many details, such as the method cannot evaluate the temperature and pressure distribution under the mudline of the subsea wellhead. Furthermore, the current methods of evaluating the temperature distribution of high-pressure wellhead are lacking with respect to the variation of wellbore temperature with location at subsea wellhead. The method proposed in this paper can be used to evaluate the safety performance of high-pressure wellhead-casing system in a thermally coupled environment.

2. Analysis Model

Fig. 1 is a two-dimensional model of a high-pressure wellhead and a schematic diagram of the loads it bears. It consists of high-pressure wellhead, rigid locking assembly, locking ring, conduit head, conduit, casing, and cement sheath. During its entire service life, it will withstand large axial and radial loads, and the high pressure wellhead is the main pressure bearing component. The welding point between it and the casing is a key fatigue hot spot. Therefore, it is of great significance to conduct thermal pressure coupling strength analysis on it.

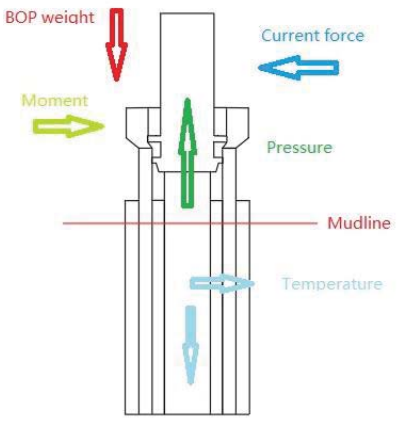

Fig.1. Two-dimensional model and load bearing diagram of high pressure wellhead.

2.1. *Wellbore axial temperature model*

Based on the laws of thermodynamics, the energy conservation equation for unit mass drilling fluid in the annulus micro element is shown in equation 1, as can be seen from Fig. 2.

$$q_a(z+dz) - q_a(z) = q_{pa-}q_f \quad (1)$$

Where q is the heat transfer per unit mass of drilling fluid, in J/Kg. The subscript *f* refers to the stratum. It can also be written as equation 2.

$$C_{fl}[T_a(z+dz) - T_a(z)] = q_{pa-}q_f \quad (2)$$

Where, C_{fl} is the specific heat of the drilling fluid, in J/(Kg·K). The energy conservation equation per unit mass of drilling fluid in the drill string microelement is shown in equation 3 and equation 4.

$$q_p(z) - q_p(z+dz) = -q_{pa} \quad (3)$$

$$C_{fl}[T_p(z) - T_p(z+dz)] = -q_{pa} \quad (4)$$

The heat transfer from the formation to the well wall (the heat transfer from seawater to the outer wall of the riser) can be expressed as equation 5 and equation 6.

$$q_{fb} = \frac{2\pi k_e}{wT_D}(T_{ei} - T_{wb})dz \quad (5)$$

$$q_{fb} = \frac{2\pi r_b U_b}{w}(T_{ei} - T_{wb})dz \quad (6)$$

The heat transfer from the wellbore to the annulus can be expressed as equation 7.

$$q_{ba} = \frac{2\pi r_c U_a}{w}(T_{wb} - T_a)dz \quad (7)$$

The heat transfer from the annulus to the drill pipe can be expressed as equation 8.

$$q_{pa} = \frac{2\pi r_p U_p}{w}(T_a - T_t)dz \quad (8)$$

Where, w is the mass flow rate of drilling fluid, in Kg/s. K_e is the thermal conductivity of the formation, in W/(m·K). r is the radius, in m. T_D is dimensionless temperature. U is the total heat transfer coefficient, in W/(m^2·K). T_{ei} is the temperature of the formation or seawater, in ℃. The subscript b refers to the outer wall of the riser, and the subscript c is the outer wall of the annulus.

$$A\frac{dT_a}{dz} = \frac{A}{B}(T_a - T_P) - (T_{ei} - T_a) \quad (9)$$

$$B\frac{dT_p}{dz} = T_a - T_P \quad (10)$$

$$A = \frac{c_{f1}w}{2\pi}\left(\frac{k_e + r_c U_a T_D}{k_e r_c U_a}\right) \quad (11)$$

$$A = \frac{c_{f1}w}{2\pi}\left(\frac{r_b U_b + r_c U_a}{r_b U_b r_c U_a}\right) \quad (12)$$

$$B = \frac{c_{f1}w}{2\pi r_p U_p} \quad (13)$$

Equations (9) and (10) are the wellbore temperature field control equations (Liu et al., 2017). Equations 11 to 13 are used to calculate the relevant parameters.

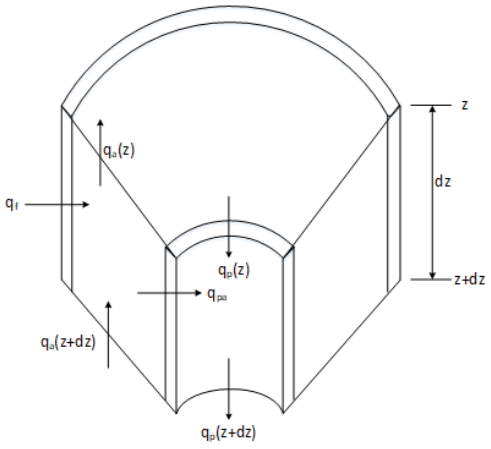

Fig.2. Heat exchange diagram of wellbore temperature field.

After determining the temperature of drill-pipe (T_p) and annulus (T_a), assuming that the annulus temperature and the inner wall temperature of the casing are the same, the temperatures of seawater and soil are known, and the temperatures of the casing, inner cement sheath, conduit, and outer cement sheath can be calculated.

2.2. *Wellbore radial temperature model*

Assuming that the temperature does not change at the junction of the two interfaces, the wellbore structure diagram is shown in Fig. 3.

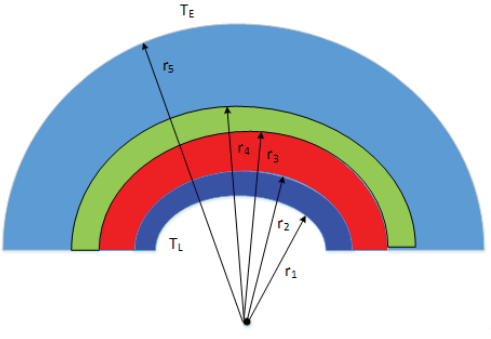

Fig. 3. Wellbore structure diagram.

Assuming that the heat transfer mode between the annular casing, cement sheath, casing, cement sheath, and seawater is a steady-state heat transfer of multi-layer cylindrical walls. The principle of series thermal resistance superposition is applied. It is assumed that the contact between the walls of

different materials is in a good state, and the average thermal conductivity of the casing, cement sheath, and conduit is respectively λ_1, λ_2 and λ_3. Thus, the heat conduction flow through the three-layer cylinder wall shown in Fig. 3 is shown in equation 14.

$$\phi = \frac{2\pi l(t_L - t_E)}{\frac{\ln(r_2/r_1)}{\lambda_1} + \frac{\ln(r_3/r_2)}{\lambda_2} + \frac{\ln(r_4/r_3)}{\lambda_3} + \frac{\ln(r_5/r_4)}{\lambda_2}} \quad (14)$$

Heat loss per unit length is shown in equation 15.

$$q_1 = \frac{2\pi(t_1 - t_4)}{\frac{\ln(r_2/r_1)}{\lambda_1} + \frac{\ln(r_3/r_2)}{\lambda_2} + \frac{\ln(r_4/r_3)}{\lambda_3} + \frac{\ln(r_5/r_4)}{\lambda_2}} \quad (15)$$

The temperature between the layers can be calculated using theoretical formulas on the condition that the inner and outer wall temperatures are known. From this, the temperature of the outer wall of the casing can be calculated as shown in equation 16.

$$T_{SO} = T_L - \frac{q_1}{2\pi}\left(\frac{1}{\lambda_1} ln \frac{r_2}{r_1}\right) \quad (16)$$

The temperature of the outer wall of the conduit is shown in equation 17.

$$T_{CO} = T_L - \frac{q_1}{2\pi}\left(\frac{1}{\lambda_1} \cdot ln \frac{r_2}{r_1} + \frac{1}{\lambda_2} \cdot ln \frac{r_3}{r_2} + \frac{1}{\lambda_3} \cdot ln \frac{r_4}{r_3}\right) \quad (17)$$

2.3. *P-Y curve calculation model*

The P-Y curve of soft clay is determined by the following formula shown in equation 18 (API RP 2A-LRFD-2019).

$$\begin{cases} \frac{P}{P_u} = 0.5\left(\frac{y}{y_c}\right)^{\frac{1}{3}} & 0 < \frac{y}{y_c} < 8 \\ P = P_u & \frac{y}{y_c} \geq 8 \end{cases} \quad (18)$$

Where, P_u is the ultimate soil resistance at the pile side, and y_c is the displacement required to reach half of the ultimate soil resistance at the pile side. P_u can be calculated by the following formula shown in equation 19.

$$\begin{cases} P_u = 3C_u + \gamma x + J\frac{xC_u}{D} & 0 \leq x < x_R \\ P_u = 9C_u & x > x_R \end{cases} \quad (19)$$

Where D is the pile diameter, γ is the effective unit weight of the soil, kN/m^3, C_u is the undrained shear strength of the undisturbed soil, kPa, and J is a dimensionless constant, typically between 0.2 and 0.5. The harder the soil is, the lower its value is. x_R is the inflection point depth of the ultimate horizontal bearing capacity, which can be estimated by the following formula shown in equation 20 (American Petroleum Institute.,2001).

$$x_R = \frac{6D}{\frac{\gamma D}{C_u} + J} \quad (20)$$

3. Analysis process

The main steps for comprehensive evaluation of high-pressure wellhead based on thermal-pressure coupling model proposed in this paper are as shown in Fig. 4. The main steps are as follows:

(1) Establish a temperature field model to determine the temperature distribution pattern of the wellbore. (2) Determine the temperature and pressure boundary conditions of the high-pressure wellhead, and create a three-dimensional finite element model of the high-pressure wellhead thermodynamic coupling. (3) Conduct strength verification and sensitivity analysis of high-pressure wellhead.

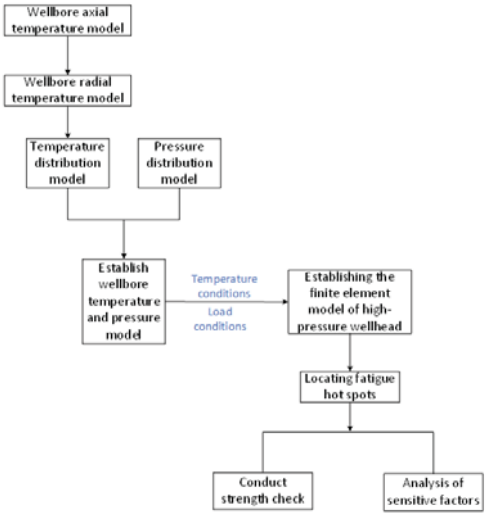

Fig. 4. Analysis process.

4. Case Study

A well in the gas field area of the South China Sea, with a water depth of 90 m. The maximum wind force is 12 degrees, and the wave height is generally 0.2~1 m. Based on the formulas of the Chinese Academy of Sciences and the Institute of Research and Levitus (Song et al., 2011), the temperature of the South China Sea water in the four seasons can be determined as shown in Fig. 5. From this, it can be seen that the temperature of seawater within the 90 m range does not change greatly within a year.

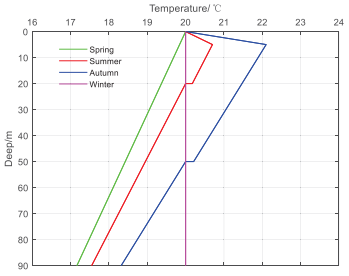

Fig. 5. Seasonal temperature distribution curve of seawater in the South China Sea.

Based on the formula in Section 2.2 and the actual temperature distribution of the high-pressure wellhead, the temperature distribution curve can be obtained as shown in Fig. 6. As can be seen from Fig. 6, the temperature distribution of the high-pressure wellhead system is between 76 and 88 ℃, with the highest annulus temperature and the lowest conduit temperature.

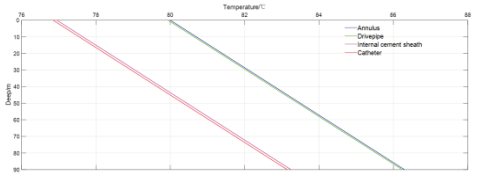

Fig. 6. Temperature distribution curve of high-pressure wellhead system.

Using Solidworks to establish a three-dimensional model of the high-pressure wellhead , and import it into ANSYS, as shown in Fig. 7. The material allocated to the high-pressure wellhead is 8630M, the material of the casing and conduit is X56M, and the material of the locking ring is 4140M, as shown in Table 1. The top of the high-pressure wellhead bears the weight of the blowout preventer and bending moment, the inside bears the working pressure. The outside of the casing head bears the current force, and the inside of the casing bears the formation pressure. The casing, conduit, and inner and outer cement sheath are set as fixed constraints. Fig. 8 is a schematic diagram of the boundary conditions of the high-pressure wellhead.

Table 1. Material parameters of key components of high-pressure wellhead.

Component	Material	Yield strength (MPa)	Thermal conductivity (w/m·K)	Coefficient of thermal expansion (℃)
HPW	8630M	552	46.6	1.22E-5
CA	X56M	390	44.7	1.17E-5
DP	X56M	390	44.7	1.17E-5
LR	4140M	896	42.2	1.37E-5

Table 2. Soil properties.

Layer	Deep Top/ m	Deep Bottom/ m	Effective gravity /(kN·m^{-3})	Design shear strength /kPa
1	0	1.6	8.6	1-13
2	1.6	5.5	8.6	13-20
3	5.5	11.8	8.1	20-50
4	11.8	21.3	8.3	50-72
5	21.3	23.3	8.2	50-72
6	23.3	28.3	8.3	50-72
7	28.3	40.5	8.7-9.9	72-82

According to the P-Y curve calculation model and soil properties (see table 2), the nonlinear spring stiffness obtained is shown in Table 3. Add the nonlinear spring stiffness to the part below the mudline to establish a high-pressure wellhead assembly, as shown in Fig. 7.

Table 3. Material parameters of key components of high-pressure wellhead.

group indication	Nonlinear spring stiffness (kN/m)
1	11.24
2	27.88
3	36.71
4	73.90
5	101.92
6	104.92
7	116.67

Fig. 7. Assembly drawing of high-pressure wellhead.

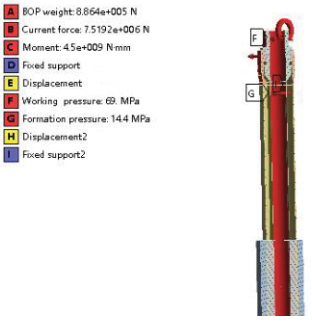

Fig. 8. Schematic Diagram of High Pressure Wellhead Boundary Conditions.

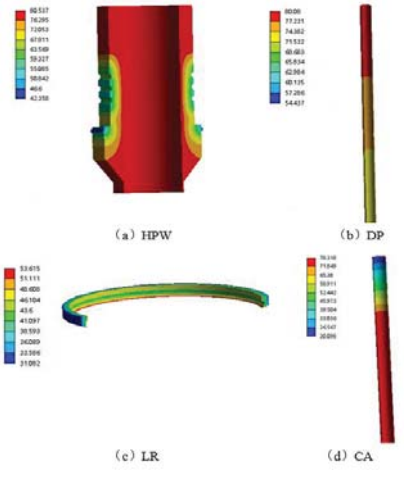

Fig. 9. Temperature distribution chart of high-pressure wellhead.

Fig. 9 shows the cloud chart of temperature distribution at the subsea wellhead. Fig. 10 shows the equivalent stress chart of the key pressure bearing components of the high-pressure wellhead obtained under the coupled model. It can be seen that the maximum equivalent stress of the locking ring is 513.88 MPa, which occurs at the contact surface matching the high-pressure wellhead. The maximum equivalent stress of the high-pressure wellhead is 433.64 MPa, which occurs at the contact surface matching the high-pressure wellhead with the locking ring and at the casing weld. The maximum equivalent stress of the casing is 284.12 MPa, which occurs at the position welded to the high-pressure wellhead. Without considering temperature, the maximum equivalent stress of the locking ring is 208.12 MPa, the maximum equivalent stress of the high-pressure wellhead is 306.89 MPa, and the maximum equivalent stress of the casing is 54.89 MPa. Which means that the equivalent stress of the locking ring increases by 2.47 times, the equivalent stress of the high-pressure wellhead increases by 1.41 times, and the equivalent stress of the casing increases by 5.18 times.

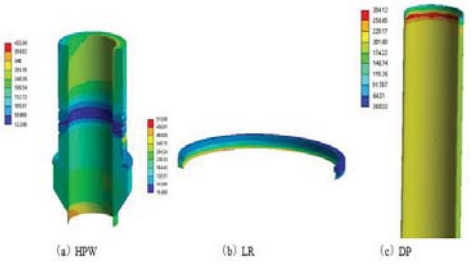

Fig. 10. Equivalent stress chart of high-pressure wellhead.

Table 4. Safety factor for key components in High Pressure Wellhead.

Component	Maximum temperature (°C)	Yield strength (MPa)	Maximum stress (MPa)	Safety factor
HPW	80.54	552	433.64	1.27
LR	53.62	896	513.88	1.74
DP	80.08	390	284.12	1.37

As can be seen from Table 4, the safety factors for key pressure-bearing components in high pressure wellhead are all greater than 1.2 in high temperature environment. Fig. 11 shows the cloud chart of deformation distribution at the subsea wellhead.

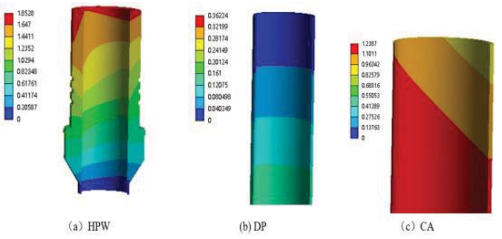

Fig. 11. Cloud Chart of Deformation of high pressure Wellhead System.

Bending moment can have a severe impact on high-pressure wellhead systems. The effects of different bending moments on high-pressure wellhead and locking ring are explored (see Fig. 12). It can be found that, with the increase of the bending moment, the equivalent stresses of the high-pressure wellhead and the locking ring show a linear increase trend. When the bending moment increases from 300,000 N·m to 600,000 N·m, the equivalent stress of the locking ring increases from 421.83 MPa to 492.61 MPa, increasing to 1.17 times of the original value. The equivalent stress of the high-pressure wellhead increases to 1.08 times of the original value. Compared with the model without considering the coupling factor, the equivalent stress of the high-pressure wellhead is higher in this model. The results is conservative.

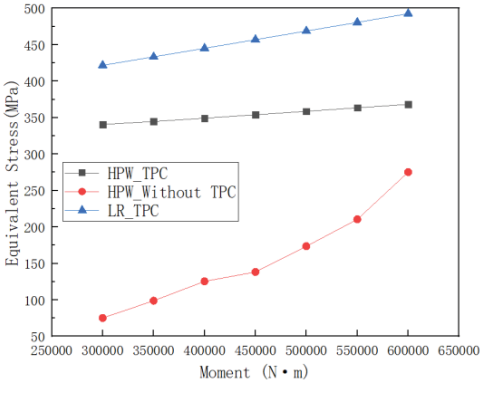

Fig. 12. Influence of bending moment on high-pressure wellhead and locking ring.

The equivalent stress variation trends of high-pressure wellhead, casing, and locking ring corresponding to different time nodes at 20 ℃, 50 ℃, and 80 ℃ were investigated (see Fig.13).

It can be seen that, under the temperature conditions of 50 ℃ and 80 ℃, the equivalent stress of the high-pressure wellhead does not change significantly within 0.9 month. However, it increases significantly between 0.9 and 1.2 months, then remains basically unchanged. The locking ring has the same pattern of change but the opposite trend. Obviously, with the increase of service time, the thermal expansion and contraction effects of materials caused by temperature will become less significant. While, the equivalent stress at 50 °C is the lowest for the casing, because the temperature difference between the inside and outside of the casing is minimal at this operating ambient temperature.

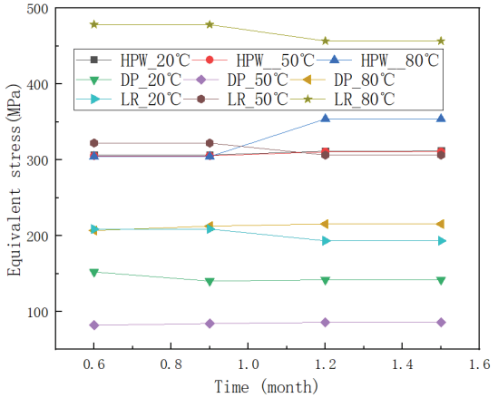

Fig. 13. Equivalent stress curves at different times and temperatures.

5. Conclusion

In this paper, a temperature distribution model of the subsea wellhead is established, from which a thermodynamic coupling model of the key pressure-bearing components of the high-pressure wellhead is built. The effects of temperature and bending moment on the equivalent stress of the pressure-bearing components of subsea wellhead are analysed, and the safety factor is calculated. The main conclusions are as follows:

(1) A method for determining the axial and radial temperature distribution of the wellbore was developed. The wellbore temperature distribution curve was obtained from the high-pressure wellhead to a total of 90 m below the mudline.

(2) Under the effect of thermal-pressure coupling, the equivalent stress of the main components of the high-pressure wellhead are all increasing significantly, with the largest increase in the casing. The high-pressure wellhead has higher axial

deformation due to heavy pressure, while the casing and catheter have higher radial deformation under the action of internal and external temperatures difference.

(3) Under the effect of thermal-pressure coupling, sudden changes in temperature within a short time frame will lead to the existence of varying degrees of increase in the maximum equivalent stress. As the service time increases, the temperature-induced thermal expansion and contraction effect of the material becomes less pronounced due to the gradual stabilization of the internal and external temperatures.

Acknowledgement

This research is supported by National Key Research and Development Project (2022YFC2806101, 2022YFC2806504-1). The authors will be grateful for the reviewers' and editor's helpful comments.

References

Yingying Wang, Zhihuang Chen, Qing Yan., 2022. A dynamic failure analysis methodology for fault diagnosis of fatigue cracks of subsea wellhead connectors with material aging. 159, 36-52.

Song Deng, Yali Liu , Panglu Jiang., 2019. Simulation and experimental study of deepwater subsea wellhead-shallow casing deflection considering system mass force. Ocean Engineering. 187, 1-10.

Xu Liu, Yongliang Wu, Wenxue Zhang., 2016. Fatigue Life Analysis of the Subsea Wellhead, Offshore Oil. 36(4), 101-107.

Yufang Li, Hongli Su, Wei Jiang., 2023. Sealing performance of subsea wellhead connector under thermal-structural coupling. Ocean Engineering. 270, 1-14.

Yuanjiang Chang，Jian Wang，Jingqi JI., 2019. A semi decoupled analysis model of subsea wellhead based on local equivalent method., Journal of China University of Petroleum(Edition of Natural Sciences), 43(3), 129-137.

Yongliang Wu, Xu Liu. 2018. Strength Analysis of Subsea Wellhead Based on ABAQUS and MOSES. Offshore Oil. 38(03), 75-82.

Yingying Wang, Zhong Li, Wentao Luo., 2022. Fatigue life prediction method for subsea wellhead welds based on the nonlinear fatigue accumulation model. Ocean Engineering. 248, 1-15.

Jiayi Li, Yuanjiang Chang, Zixiang Xiu., 2020. A local stress-strain approach for fatigue damage prediction of subsea wellhead system based on semi-decoupled model. Applied Ocean Research. 102, 1-9.

Na Qiu, Xiuquan Liu, Zhaowei Liu., 2022. Dynamic stability evaluation of subsea wellhead based on fully coupled model. Ocean Engineering, 257, 1-12.

Wei Yan, Zijian Chen, Jingen Deng., 2015 Numerical method for subsea wellhead stability analysis in deepwater drilling. Ocean Engineering, 98, 50-56.

Anders Wormsen , Arne Fjeldstad , Finn Kirkemo., 2017. Fatigue analysis of low alloy steel forgings used in the subsea industry. International Journal of Fatigue 96, 43–66.

Baoping Cai, Hongyan Fan, Xiaoyan Shao., 2021. Remaining useful life re-prediction methodology based on Wiener process: Subsea Christmas tree system as a case study 151, 1-13.

Yanping Zhang, Baoping Cai, Yiliu Liu., 2021. Resilience assessment approach of mechanical structure combining finite element models and dynamic Bayesian networks. 216, 1-11.

Xiangkun Meng, Guoming Chen, Jingyu Zhu., 2022. Application of integrated STAMP-BN in safety analysis of subsea blowout preventer. Ocean Engineering, 258, 1-11.

Yanbin Wang, Deli Gao, Jinduo Wang., 2022. Investigation on influence of temperature and pressure on fatigue damage of subsea wellhead in deepwater drilling. Journal of Petroleum Science and Engineering. 212, 1-15.

Jinge Liu, Honghai Fan, Liang Zhu., 2017. Development of a transient method on predicting multi-annuli temperature of subsea wells. Journal of Petroleum Science and Engineering 157, 295–301.

API RP 2A-LRFD-2019.

American Petroleum Institute. API RP 16Q-2001, Recommended practice for design selection operation and maintenance of marine deilling riser system. Washington DC: American Petroleum Institute, 2001.

Xuncheng Song, Zhichuan Guan. 2011 Full transient analysis of heat transfer during drilling fluid circulation in deep-water wells. Acta Petroleum Sinica, 32(04), 704-709.

List of Abbreviations

Abbreviation	Definition
BOP	Blowout Preventer
HPW	High Pressure Wellhead
DP	Drive Pipe
CA	Catheter
LR	Lock Ring
TPC	Thermal Pressure Coupled